ELSEVIER

Journal of Neuroscience Methods 108 (2001) 131–144

JOURNAL OF NEUROSCIENCE METHODS

www.elsevier.com/locate/jneumeth

Application of neurosonography to experimental physiology

Paul W. Glimcher [a,*], Vivian M. Ciaramitaro [a], Michael L. Platt [b], Hannah M. Bayer [a], Michael A. Brown [a], Ari Handel [a]

[a] *Center for Neural Science, New York University, 4 Washington Place, 809 New York, NY 10003, USA*
[b] *Department of Neurobiology, Duke University Medical Center, Durham, NC 27710, USA*

Received 26 March 2001; received in revised form 4 April 2001; accepted 4 April 2001

Abstract

When Horsley and Clark invented the stereotaxic technique they revolutionized experimental neurobiology. For the first time it became possible to repeatably place experimental or surgical probes at precise locations within the skull. Unfortunately, variations in the position and size of neuroanatomical structures within the cranium have always limited the efficiency of this technology. Recent advances in diagnostic medical ultrasonography, however, allow for the real-time visualization of anatomical structures, in some cases with resolutions of up to 150 μm. We report here that commercially available ultrasonographs can be used in the laboratory to generate real-time in vivo images of brain structures in both anesthetized and awake-behaving animals. We found that ultrasonic imaging is compatible with many types of experimental probes including single neuron recording electrodes, microinjection pipettes, and electrodes for producing electrolytic lesions. Ultrasonic imaging can be used to place, monitor and visualize these probes in vivo. In our hands, commercially available ultrasonic probes designed for pediatric use allowed us to visualize anatomical structures with sub-millimeter resolution in primate brains. Finally, ultrasonic imaging allowed us to reduce the risk of accidentally damaging major blood vessels, greatly reducing the incidence of stroke as an unintended complication of an experimental neurosurgical procedure. Diagnostic ultrasound holds the promise of reducing the uncertainty associated with stereotaxic surgery, an improvement which would significantly improve the efficiency of many neurobiological investigations, reducing the number of animal subjects employed in this research. While this demonstration focuses on sonographic imaging in non-human primates, similar advances should also be possible for studies in other species, including rodents.

Keywords: Sonography; Neuroanatomy; Physiology; Primate

1. Introduction

1.1. Techniques for structural localization

Before the early 1900s neurobiological experiments conducted within the crania of living animals were limited in scope. Landmarks like the sutures between the bones of the skull could be used to guide the placement of probes (cf. Fritsch and Hitzig, 1870), but conducting accurate experiments in deep brain nuclei was essentially impossible because probes could not be placed repeatably at anatomical locations of interest. As a result, Horsley and Clarke revolutionized neurobiology when they developed the stereotaxic technique because it permitted anatomically repeatable studies of both cortical and subcortical structures within the living brain. As they put it: "In short, instead of employing the usual method of endeavoring to project the detailed structure of the interior of the encephalon onto the surface of the head, we measure the position of the deep part of the brain by their relation to three sectional planes" (Horsley and Clarke, 1908). Since the introduction of this technique in 1908 it has become a ubiquitous component of neurobiological research in animals and an essential tool for neurosurgical procedures in humans.

While the invention of the stereotaxic technique was undoubtedly one of the seminal advances in modern neurobiology, it has placed limits on the productivity and efficiency of modern neurobiological research. At

* Corresponding author. Tel.: +1-212-9983904; fax: +1-212-9954011.
E-mail address: glimcher@cns.nyu.edu (P.W. Glimcher).

0165-0270/01/$ - see front matter
PII: S0165-0270(01)00365-X

least three sources of variance, all of which were well known to Horsley and Clark, impose these limits. First, stereotaxic coordinates presume that all animals used for experimentation have exactly the same head size and cranial dimensions. Second, the technique assumes that neuroanatomical structures of interest lie at exactly the same three dimensional position with regard to the cranium across individuals, an assumption which is particularly violated by the idiosyncratic pattern of folding observed in the cerebral cortex of many primates. Finally, the technique assumes that a comprehensive database relating the location of a structure to the stereotaxic planes exists for each species and size of animal to be studied.

Horsley and Clarke accepted these limitations of a fixed three-dimensional coordinate system because there was no non-invasive way to visualize deep brain anatomical structures. Over the course of the last several decades, however, a number of imaging techniques have been developed which permit the direct visualization of anatomical structures in living brains. These techniques raise the possibility that, instead of employing the usual method of projecting the detailed structure of the brain into a set of three dimensional coordinates and then locating experimental probes within those coordinates, one could achieve direct, intrasurgical, visualization of both experimental probes and anatomical structures of interest.

Two techniques in particular stand out as potentially useful: Magnetic Resonance Imaging and Ultrasonography. Current magnetic resonance imaging holds exceptional promise in this regard, allowing brain structures in primates to be imaged non-invasively with resolutions better than 0.5 mm. A number of technical constraints, however, limit the utility of this technique in the laboratory. First, the technique is expensive and requires hardware that is difficult to use in a surgical or laboratory setting. Second, the magnetic fields emitted by the imager are incompatible with many of the surgical probes used in neurobiological research. Finally, the technique is difficult to use in conscious animals. While there is reason to believe that many of these constraints can and will be overcome (cf. Logothetis, 2000), they have until now limited MR imaging in surgical settings to the generation of subject by subject atlases that can serve as a comprehensive database relating the location of a structure to the stereotaxic planes for each individual.

Although sonographic imaging of brain structures has a long history of clinical application and would circumvent many of the constraints that face magnetic resonance imaging, ultrasonography has received very little attention from experimental neurobiologists. Clinically, ultrasound was first used to measure displacements of the midline in adult brains by placing an ultrasonic emitter outside the skull and then recording the acoustic reflections of midline cranial structures (Leksell, 1956; Gordon, 1958). Because the efficiency of this technique was limited by the acoustic opacity of the skull (White and Curry, 1975; White et al., 1978), a number of researchers (cf. Kikuchi et al., 1957) began to examine intracranial pathologies ultrasonically through burr holes made in the skulls of adult patients. The development of non-invasive Computed Axial Tomography in the 1970s, however, essentially ended this line of clinical research in adults. At that time the focus of neurosonographic research shifted to studies in human neonates, whose cranial bones are not yet fused or fully mature. Neonatal and pediatric brain sonography has continued to develop and is now used routinely in the clinic with resolutions that can approach 0.3 mm.

Within the setting of experimental neurobiology, sonography has received almost no attention even though there has been at least one major technical advance in recent years. Using very high frequency ultrasound Turnbull and colleagues have developed an ultrasonic microscope (Turnbull et al., 1995; Olson et al., 1997) for imaging fetal mouse brains and microinjection probes with an accuracy in the micron range. These observations led us to ask: if a portion of the skull were removed chronically, could ultrasound be used in the laboratory to image brain structures and experimental probes simultaneously in adult animals? Since ultrasonic probes are small, unobtrusive and relatively inexpensive, the technology should be broadly compatible with existing techniques for the neurobiological study of anesthetized and behaving animals. Used in this way, ultrasonic imaging might allow experimental scientists to overcome many of the limitations of a traditional stereotaxic approach. We report here that clinical ultrasound can, in fact, be easily adapted for use in an experimental physiology laboratory and that the technique significantly improves the speed and accuracy of many common experimental procedures. A preliminary report of this technique has been presented (Glimcher et al., 1999).

1.2. Overview of sonography

Sonographic imaging is accomplished by emitting an intense pulse of high frequency sound into a tissue of interest and then determining the intensity and arrival time of returning acoustic echos generated by tissue interfaces that are reflectors or scatterers. To achieve high resolution along the scanned path of an emitted ultrasound pulse it is essential to use high frequencies of sound for which the wavelength is small because the wavelength determines the spatial uncertainty of the returning echo. In practice, most commercial sonographs employ emitted pulses in the 2–20 MHz range which provide theoretical resolutions along the path of the sound wave of 1.54–0.15 mm (assuming a sound

velocity in tissue of 1.54 mm/μs; Kremkau, 1998). Higher frequencies provide higher resolution. This advantage of higher frequencies is offset, however, by the fact that higher frequencies are attenuated more quickly as they pass through tissue (typically at 1 dB/cm/MHz; Kremkau, 1998). While 2 MHz pulses can be used to image tissue at distances greater than 20 cm, 10 MHz pulses are currently limited to use in imaging structures within 3–6 cm of the probe (depending on the sensitivity of the receiver). For a given application, then, one must select an imaging frequency which provides adequate resolution at an acceptable depth. Thus, a tradeoff exists suggesting that different imaging frequencies will be appropriate for neuroanatomical imaging in different species; small animals like rats will require high frequency probes while larger animals will require lower frequency probes. For use in old world monkeys, we have found that an imaging frequency of 7.5 MHz is ideal, providing resolutions along the imaging axis of the probe of 400 μm while allowing imaging of all tissue within the cranial vault of the monkey brain.

Commercial sonographs use an array of many highly focused co-planar emitters, activated in sequence, to generate what are essentially acoustic scan lines, each of which resolves the distance to any acoustically significant boundaries encountered along the path of the emitted pulse. A series of the co-planar scan lines can thus resolve anatomical structures within a plane, or section, through the tissue of interest. Vertical resolution is in principle set by the frequency of the emitted pulse, while horizontal resolution (perpendicular to the imaging axis of the probe) is determined in principle by the spacing between scan lines and the efficiency with which scan lines can be focused. In practice, horizontal resolution is significantly lower than vertical resolution.

From a series of adjacent scan lines a gray scale, or *B-mode*, image is computed which plots the *x*-*y* coordinates of acoustically significant boundaries within the imaged plane, where the brightness of each pixel essentially encodes the intensity of the acoustic signal reflected at that depth along the scan line[1]. Finally, Doppler shift (a shift in the frequency of the returning echo due to motion of the reflecting object) can be used to identify arteries and veins within the living brain (Gill and Kossof, 1977; Fitzgerald and Drumm, 1977). Essentially all of the macroscopic vasculature within an imaged plane can be visualized because the turbulently flowing blood within the vasculature produces a range of doppler shifts from any vessel which are easily detected by the receiving probe. Doppler signals can be presented in two forms, either as an encoding of the mean magnitude of the doppler shift at each pixel, or an encoding of the RMS power of the doppler induced spectral broadening. Typically these data are presented as color images overlayed on gray scale B-mode images.

1.3. Applications

In our laboratory we have employed sonographic imaging in several experimental settings: (1) To demonstrate the efficiency of the technique we have generated a sonographic atlas of the macaque brain in coronal and sagittal section. (2) To test the technique in awake-behaving animals we have generated sonographic atlases of 1 cm patches of cortical tissue lying beneath standard recording cylinders (Platt and Glimcher, 1997) in awake-behaving monkeys. (3) To localize single neuron recording electrodes in the cortices of anesthetized animals we have simultaneously imaged electrodes and anatomical structures during electrophysiological experiments. (4) To guide the placement of electrolytic lesions we have visualized lesioning electrodes and anatomical structures in anesthetized animals. We have then used B-mode and doppler imaging to monitor lesion formation. (5) To guide the injection of neuroanatomical tract tracers through glass micropipettes into ventral cortical regions (Suzuki and Amaral, 1994) we have visualized glass pipettes and anatomical structures in the brains of anesthetized animals. (6) To guide the placement of single neuron recording electrodes in awake-behaving monkeys along trajectories that minimize vascular injury we have used combined B-mode and doppler ultrasonography to place recording electrodes in a number of brain areas including the substantia nigra and the superior colliculus (Handel and Glimcher, 1999).

2. Methods

2.1. General techniques

We used two commercially available diagnostic ultrasound imagers with multi-frequency probes designed for pediatric brain imaging through the neonatal fontanel. The images presented here were generated using a General Electric Logic 700 Pro equipped with a 618c probe. We also successfully used a Toshiba PowerView 7000 equipped with a 10 MHz probe. The GE 618c probe, shown in Fig. 1, has an 8 mm (wide) by 12 mm (long) footprint (although the entire probe face need not be used) and was used exclusively at a center frequency of 7.5MHz. Because most commercial ultrasound machines provide limited mechanisms for data export, we elected to capture the raw video output from these machines with a commercial grade video digitiza-

[1] Of course sonography involves a large number of techniques, and a number of artifacts ranging from acoustic refraction to heightened absorption produce distortions in the image, but these issues are beyond the scope of this presentation. For a full treatment of sonographic imaging the reader is refered to: Kremkau (1998).

Fig. 1. Sonographic probe. A General Electric 618c sonographic imaging probe is shown along side a standard Crist (Crist et al., 1988) recording chamber and a plastic access chamber that we designed. Our cylindrical chamber was made of rigid plastic and this model had an inside diameter of 25 mm and a height of 6 mm. The probe emitters are arranged in a curved array along the bottom of the sonographic probe. We have successfully used this probe to image fine anatomical structure through these implantable cylindrical chambers.

tion board installed in a PowerMac G3 computer. Video data was then processed off-line[2]. All of the images shown here were made on macaque monkeys (*mulatta*, *nemestrina*, and *fascicularis*) weighing between 3 and 12 kg. All experimental procedures were approved by the New York University Institutional Animal Care and Use Committee and complied with the PHS *Guide for the care and use of animals*. While it is beyond the scope of this presentation to review the standard techniques of clinical ultrasonic imaging, we developed several techniques specific to experimental intracranial imaging. We review each of these techniques below.

2.2. Opening a cranial aperture for imaging

The footprint of the imaging probe largely controls the size of the cranial aperture needed for efficient imaging. If the aperture is too small, this results in acoustic scatter from the ultrasonic emitters overlying the bone itself, which appears on the sonographic im-

[2] Although high quality image processing is completed within the ultrasonograph, almost none of the proprietary data processed within the ultrasonic images is available to users in a more direct form than as image data. General Electric does, however, offer direct access to data gathered by the probe on some of its machines.

age as noise. Further, limiting the size of the aperture limits the number of vertical scan lines that pass through the tissue. Because many probes can dynamically adjust the inter-scan line spacing to produce images of arbitrarily selected width, reducing the width of the cranial aperture effectively limits the resolution of the image. In the images presented here we used apertures that typically ranged from 8 to 20 mm in diameter and a probe with a footprint of about 12×8 mm. We found that a clean, smooth edge to the aperture minimized scattering at the aperture edge. Our preferred aperture for use with the GE 618c probe was a craniotomy 12 mm or larger in diameter made with a hand drill or trephine. Producing an irregularly edged aperture with surgical rongeurs tended, in our experience, to produce unacceptable scatter. Making optimal use of the aperture requires bringing the probe as far into the aperture as possible. Placing the probe high above the aperture simply serves to restrict the effective field of view of the probe and also induces scattering artifact from the outer surface of the skull.

2.2.1. Acute studies

In experiments where animals were to be maintained in a chronically anesthetized state we often filled the craniotomy used for imaging with liquid agar, mixed slowly at a concentration of 3.75 g/100 ml and allowed to stand while mixing slowly for at least 5 min (to exclude air bubbles). The agar, once cooled to body temperature, was laid directly over the exposed dura and allowed to harden. In this condition it provided a fairly rigid cover for the craniotomy that was transparent to ultrasonic energy. We found air bubble free agar more transparent than either commercially available sonographic gel or saline.

2.2.2. Chronic studies

For chronic studies in awake-behaving animals, we permanently implanted resealable aseptic cylindrical access chambers over the imaging craniotomies. We fabricated these chambers, which had an inside diameter of either 25 or 19 mm, and a height of 6 mm, out of rigid plastic. We found that it was possible to produce clear sonographic images through these chambers for more than one year after implantation. For imaging, a thin coating of sterile mineral oil was first applied to all surfaces within the chamber. The cavity within the chamber was then filled with a precast agar plug. At the beginning of each week we cast 10–30 cm of agar in a sterile teflon pipe with the same inside diameter as the sonographic chamber and stored this pipe at 4°C. Before imaging we extruded a piece of agar from the pipe equal in length to the depth of the imaging chamber and sliced it from the precast block with a sterile scalpel. Agar plugs were removed from the imaging chambers at the end of each day because the agar was most acoustically transparent when new and degraded rapidly in the chamber.

2.3. Coupling: establishing and maintaining an efficient probe to brain interface

The most critical element for successful intracranial imaging was to maintain an efficient acoustic coupling between the brain itself and the emitter surface of the probe. One of the most critical aspects of this coupling was to insure that unwanted scatterers, like air bubbles, were as completely excluded from the sound path of the emitters as possible. We typically accomplished this with a multipart interface. First, several milliliters of saline were poured into a sterile sonographic probe cover or unlubricated condom. Saline was always poured from bottles that had been allowed to stand overnight, or had been degassed in a vacuum chamber. This was critical because it minimized the number of air bubbles in the saline which would serve as scatterers along the imaging sound path. The probe was then inserted into the condom until it was within 5 mm of the end of the probe cover. Next, the face of the probe cover was coated with sterile mineral oil. The probe cover was then brought into contact with either the agar plug or with the dura itself, which were also coated with sterile mineral oil. The probe was always positioned so that at least 1 or 2 mm of saline was interposed between the probe face and the agar or dura, preventing the rigid probe face from coming into direct contact with the dura or agar. As a final note, we also attempted to image intracranially at the end of a surgical procedure that required the resection and reattachment of the dura. Such a procedure invariably trapped air bubbles beneath the dura which degraded sonographic visualization significantly.

2.4. Optimizing neurobiological probes for visualization

Not all of the neurobiological probes used intracranially are easy to visualize sonographically. We found that standard extracellular electrodes, for example, could only be well visualized when they were advanced at an angle of about 35°, or greater, to the imaging axis of the probe. Furthermore, we found that metal electrodes insulated with glass tended to be easily visualized, while plastic insulated electrodes tended to be more difficult to image. To overcome this limitation we coated electrodes and other probes with an acrylic varnish (available at craft stores) which left a slightly roughened surface on the electrode, enhancing the sonographic image. Electrodes were marked in this manner to within 5 mm of their tips and then, when imaging, we extrapolated where the tip should be from an image of the sono-enhanced shaft of the electrode. In many cases, scatter induced by the tip of the elec-

trode was easily visible at that location. When we used pulled glass micropipettes for neuroanatomical injection studies these probes were coated with an acrylic varnish to within 10 mm of their tips. Because all modern ultrasonic imagers come with precise measurement tools it was possible to extrapolate the location of the unvisualized electrode or micropipette tip with significant accuracy.

2.5. Visualizing electrodes for chronic physiological studies

In order to localize electrophysiological recording electrodes within the brains of chronically studied awake-behaving primates, we performed two craniotomies on these animals. Over one of these craniotomies we implanted a standard recording chamber (Crist et al., 1988) and over the other we implanted a cylindrical plastic access chamber (as described above) for sonographic recording. We found that sonographic imaging was more efficient as the angle formed by the central axes of the two chambers increased. We typically achieved an adequate axial separation by placing the plastic sonographic chamber in the same fronto-parallel plane as the recording chamber, but on the contralateral side of the skull. This allowed us to produce images in the coronal plane which included electrodes advanced through the recording chamber. Although the curvature of the skull largely controls the angular separation between the two chambers under these conditions, we typically achieved an axial separation of between 25° and 50°. In practice, intrasurgical visual alignment of the plastic sonographic chamber and the standard recording chamber into the same fronto-parallel plane produced excellent results.

In order to maximize the visibility of our recording hardware within the brain we modified our electrophysiological hardware. First, we replaced our traditional electrode guide tubes (Crist et al., 1988) with guide tubes fabricated from biopsy needles designed for sonograph visualization (22 g Sono-Vu needles: E-Z-EM. Westbury, NY). These needles are coated, drilled, and beveled for maximum sonographic visibility and we found that the tips of these needles were easily visible during neurosonography. Second, we sheathed our electrodes in stainless steel needle tubing [15] which served as a bushing to which the electrode was rigidly attached and which moved freely within the guide tube. The final 10 mm of this tubing, from which the electrode tip projected, was heavily abraded to produce a rough and irregular surface that promoted acoustic scattering. The distance that the electrode projected out from this roughened bushing was measured to an accuracy of at least 0.25 mm. These modifications allowed us to visualize the guide tube and the bushing as it was extended beyond the guide tube. Using these modifications it was possible to extrapolate the location of the electrode tip and on some occasions to visualize the electrode tip directly. We found that the ability to identify the location of the electrode tip at each recording site reduced the anatomical uncertainty associated with chronic recording studies and should reduce the need to perform histological analyses in the future.

3. Results

3.1. Anatomical images: whole brain

Fig. 2 presents anatomical images of a living brain of an anesthetized macaque monkey generated through a craniotomy approx. 15 mm wide along the mediolateral axis that extended rostro-caudally 30 mm. The 15 mm width of the craniotomy allowed our probe to image the entire brain in coronal section. The 30 mm length allowed us to produce coronal images at many rostro-caudal levels. Panel A shows coronal sections of doppler blood flow and B-mode images adjacent to cut slabs taken from the same brain post-mortem. Note that the B-mode panels (center) allow identification of most major sulcal boundaries, the lateral ventricles (marked by the acoustically reflective ventricular parenkyma which appear as the white sulcal boundaries in the sonographic image), and a number of subcortical and cerebellar structures. The doppler panels (left) show the major vascular features in these areas including the basilar artery and the inferior sagittal sinus. Panel B shows a sagittal section from this same brain. The major cortical sulci, the rostral boundary of the thalamus and a number of brainstem structures are all visible in the B-mode image. The doppler image reveals the Circle of Willis, the Anterior Cerebral Artery, and a number of sub-callosal vessels.

3.2. Monitoring acute physiology: cortical area MT

Fig. 3 presents a B-mode sagittal section through areas MT and MST (Gegenfurtner et al., 1994) adjacent to the superior temporal sulcus and caudal to the lateral sulcus. The B-mode image has been focussed and magnified to provide a high resolution image of the MT/MST region. Note the region of increased reflectivity at the posterior edge of the superior temporal sulcus. This is the tip of a glass insulated tungsten electrode which passes out of the imaging plane towards the left side of this image. The mediolateral position of the probe has been adjusted to visualize the most caudal point of reflection on the electrode. Inset below is a physiological waveform recorded from this electrode while the sonograph generated this anatomical image and while a broad frequency visual stimulus was drifted across the visual field of the monkey. Inset

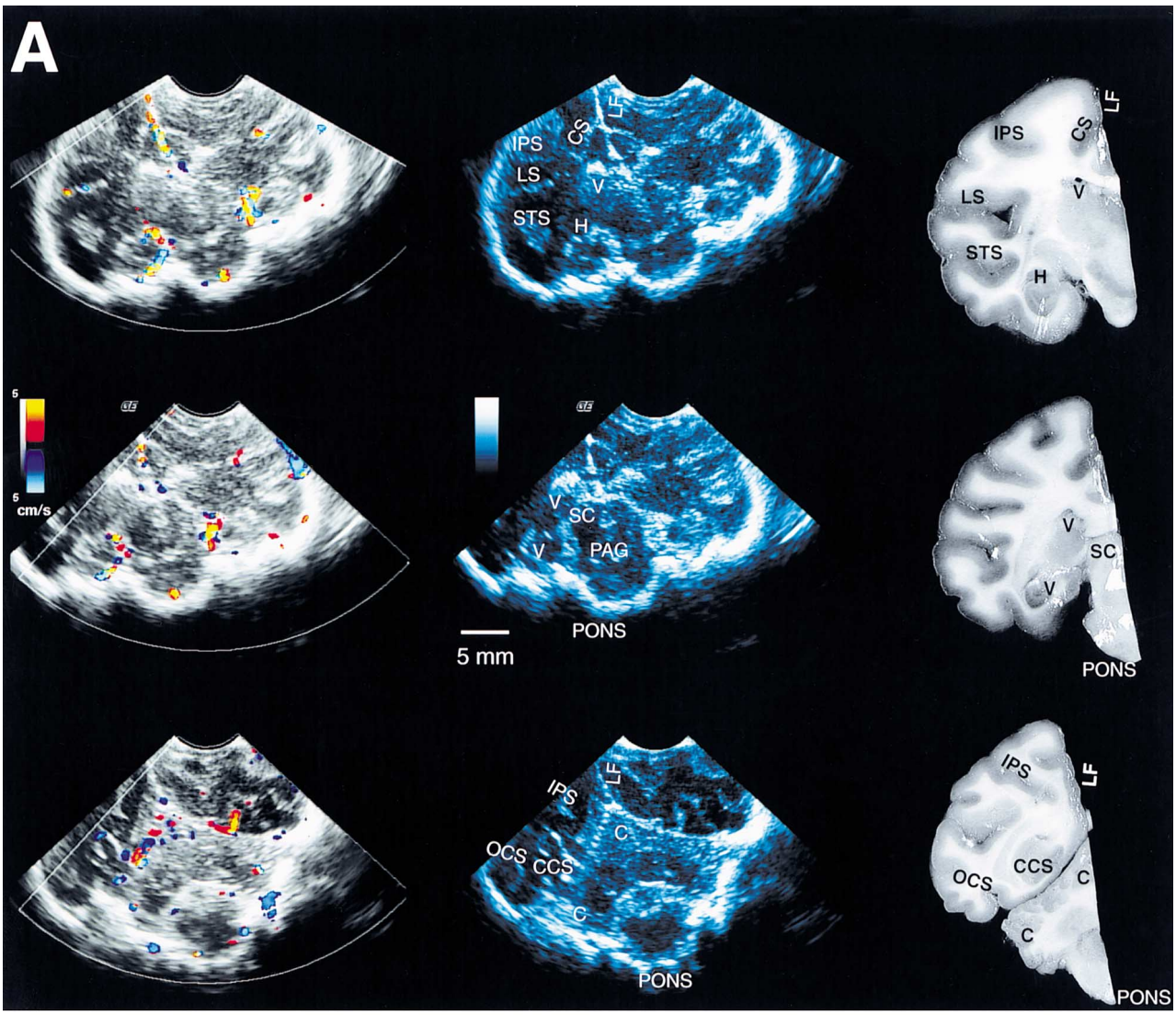

Fig. 2.

above is a sagittal section stained for myelin showing the standard sulcal patterns in this area[3]. A 2 min quicktime movie of this recording session can be downloaded from our website: http://www.cns.nyu.edu/~glimcher.

3.3. Lesion localization: cortical area MT

Fig. 4 shows a time-series of images gathered at 1 s intervals before and during the formation of an electrolytic lesion in cortical area MT. The upper panels (A) present B-mode images. The lower panels (B) present the magnitude of the doppler power spectrum (power doppler imaging) in color as an overlay on B-mode images. The lesion was produced by passing a 5 μA cathodal current through the electrode for 5 s. The lesion began immediately after the images presented in the left most panels were gathered. The lesion itself appears as a growing area of high reflectivity at the tip of the electrode that reaches a stable size by the third image (upper yellow arrow). We found that this area of high reflectivity persisted at this location for several minutes in the B-mode image. (Presumably this region of high reflectivity was produced by bubble formation near the electrode tip.) Panel B shows power doppler images of the lesion. Note the vessel within the sulcus and above the electrode which is present before the lesion. Immediately after the cathodal current is activated (second panel) a transient broadening of the spectrum of the ultrasonic echo indicates movement at the lesion site (lower yellow arrow) which persists for less than a second.

3.4. Anatomical injections: cortical area TF

Fig. 5 shows a B-mode image of a coronal section through the brain of an anesthetized monkey which includes the hippocampus and parahippocampal cortex. The solid white line seen on the right side of the B-mode image (marked with a yellow arrow) is a pulled glass pipette coated, to within 10 mm of the tip, with an acrylic varnish. The dotted yellow line and yellow cursor marks the estimated location of the fine tip itself, based on a pre-injection measurement of the distance from the end of the acrylic coating to the tip of the pipette. The pipette was used to inject biotinylated dextran amine (BDA) into the medial subdivision of area TF of the parahippocampal cortex. The left panel shows a post-mortem coronal section immunologically stained for BDA, showing the recovered location of the injection with an inset of the injection site. The black arrow marks the track of the injection pipette. The inset darkfield photomicrograph shows the injection site in area TF at higher magnification.

3.5. Chronic electrophysiology in awake-behaving primates: superior colliculus

Fig. 6 shows B-mode and doppler images of a sonographically visible guide tube placed just above the superior colliculus of an awake-behaving monkey. The left panel shows a B-mode coronal section at the level of the superior colliculus imaged at $\sim 25°$ to the left of vertical. Visible on the left side of the image are all of the major cortical sulci in this area and the lateral ventricle. Beneath these the outer boundary of the brainstem can be seen. On the right side, entering at an angle of 25° to the right of the longitudinal fissure (LF), and hence at 50° to the right of vertical in the image, is a sonographically visible guide tube through which an electrode will be advanced. Note that the guide tube has been positioned ~ 1 mm above the superior colliculus and that at this location it compresses the collicular surface. We found that by repeatedly extending and retracting the guide tube we could observe a systematic compression and re-expansion of the collicular surface. The middle panel replots this image but overlays an anatomical line drawing and abbreviations for many of the anatomical features visible in the image. The right panel plots a doppler blood flow image which

Fig. 2. Sonographic Sections: Monkey Brain. Sonographic images of a macaque brain taken through a 15 mm wide and 30 mm long imaging craniotomy. The animal was anesthetized while these images were made and was then perfused. The whole brain was then cut in the mid-sagittal plane. Coronal slabs were cut from one hemisphere and photographed for panel A. Sagittal slabs were cut from the other hemisphere and photographed as shown in panel B. All sonographic images were made with a GE 618c probe operating at a center frequency of 7.5 MHz and with four depth foci distributed evenly through the image. Sixty-six density levels are encoded in each image. (A) Coronal images. Left panels plot doppler blood flow. The scale bar shows the relationship between color and the speed of blood flow towards or away from the probe. Particularly visible in these images are the basilar artery at the very bottom of the brain and the mid-sagittal sinus at the top, particularly in the uppermost image. Middle panels plot color enhanced B-mode images. The right panels plot, for comparison, slabs cut from the same brain shown in approximately the same anatomical plane. (B) Sagittal images. Same conventions as in panel A. Abbreviations: C, cerebellum; CC, corpus callosum; CCS, calcarine sulcus; CS, cingulate sulcus; H, hippocampus; IPS, intraparietal sulcus; ISS, inferior sagittal sinus; LF, longitudinal fissure; LS, lateral sulcus; OCS, inferior occipital sulcus; PAG, peri-aqueductal gray; SC, superior colliculus; STS, superior temporal sulcus; V, lateral ventricle.

[3] The histological micrograph shown here was kindly provided by Professor W.T. Newsome of the Howard Hughes Medical Institute and Stanford University.

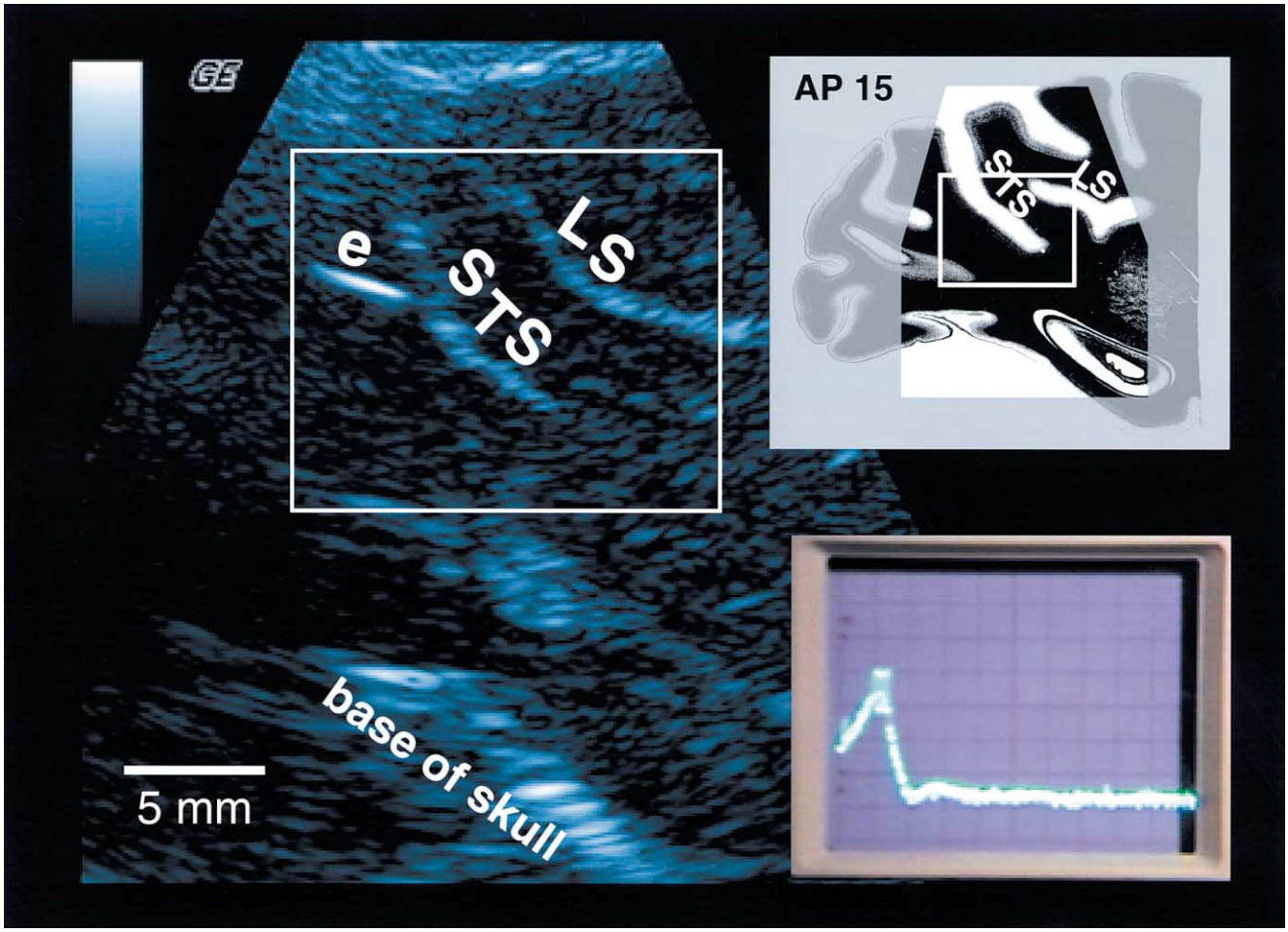

Fig. 3. Sonography during acute physiology. Sonographic image of a macaque brain in sagittal section taken through a 10 mm diameter craniotomy made in an anesthetized animal. GE 618c probe was used operating at a center frequency of 7.5 MHz, near maximal zoom magnification with foci centered on the superior temporal sulcus (STS). The letter 'e' marks the distal end of a tungsten electrode insulated with glass. The tip of this electrode lies within the *physiologically defined* cortical area MT, caudal to the sulcus. The lower inset shows the electrophysiological waveform recorded from this electrode as the sonographic image was obtained. The action potential pictured on the oscilloscope was produced by a cell at the electrode tip. The upper inset shows a sagittal section, approximately aligned with the sonographic image, stained for myelin (courtesy of W.T. Newsome and colleagues). Abbreviations: e, electrode; LS, lateral sulcus; STS, superior temporal sulcus.

shows the midsagittal vasculature, vessels within the intraparietal sulcus, and several deep brainstem vessels. The green dotted line plots the estimated trajectory that would be taken by an electrode advanced through the guide tube. We found that an electrode advanced through the guide tube did travel along this predicted trajectory. The lower green cross estimates the point at which the electrode would cross the midline. On the bottom right the sonograph displays the total length of the dotted line.

3.6. Resolution

In order to estimate the resolution of our sonographic images, we determined the size of the image produced by an object smaller than the theoretical resolution limit of our equipment. By knowing the size of the image generated by an object that was effectively a point, we could estimate the minimum spatial separation at which two different objects could be resolved. To accomplish this, we measured the horizontal and vertical dimensions of the echos (measured as the width and height of the echo at 6 dB attenuation) returned by the tips of tungsten micro-electrodes (or abrasions along the sides of the electrodes) used for extracellular recording. We made these measurements at a range of distances to estimate how resolution was effected by the depth of brain tissue through which the imaging pulse traveled. We used this approach because previous studies of sonographic resolution have successfully employed this method to estimate resolution (Suhm et al., 1998).

Fig. 7 plots resolution as a function of distance along both the vertical and horizontal axes of the imaging probe. Each point is the average of between three and seven observations. At depths of up to nearly 35 mm the

vertical size of the echo returned by the electrode was 0.4 mm or less. These images were produced with a 7.5 MHz imaging pulse which has a theoretical spatial uncertainty, imposed by the pulse wavelength, of ~ 0.4 mm. Our probe thus achieved an axial resolution near the theoretical limit. At these same depths, however, the horizontal size of the echo was 1 mm or more. These data suggest that at distances of up to 35 mm a 7.5 MHz probe can be used to resolve the axial position of a neurobiological probe with a vertical accuracy of better than 0.5 mm, but with a horizontal accuracy that is significantly worse at these same distances. However, because one can orient the probe at many angles to the underlying tissue, it is often possible to align the vertical axis in a way that maximizes the resolution with which a structural boundary of interest is imaged.

Both horizontal and vertical accuracy degrade as the distance between the probe and the electrode increases towards 50 mm. In practice we found both the horizontal and vertical resolution to be adequate for the intrastructural placement of neurobiological probes at distances of up to 35 mm under essentially all conditions. At greater distances we found that the axial resolution was still adequate for physiological applications, even though the horizontal uncertainty limited the utility of the technique at this frequency.

4. Discussion

Until recently, classical stereotaxic surgery was the only technique available for the placement of surgical probes at repeatable locations within the living brain. The inherent limitations of stereotaxic surgery have, however, always restricted the efficiency of neurobiological experiments. In vivo sonographic imaging is one technique that holds the promise of overcoming these limitations and providing anatomical images that can guide neurobiological research in real-time and at low cost. Although sonography also imposes limits on the efficiency of neurobiological research, by judiciously selecting an imaging strategy it is possible to use sonography to achieve a significant improvement in the speed, accuracy and repeatability of many neurobiological procedures.

The trade-off between imaging depth and imaging resolution is perhaps the most important constraint that must be considered when evaluating sonographic

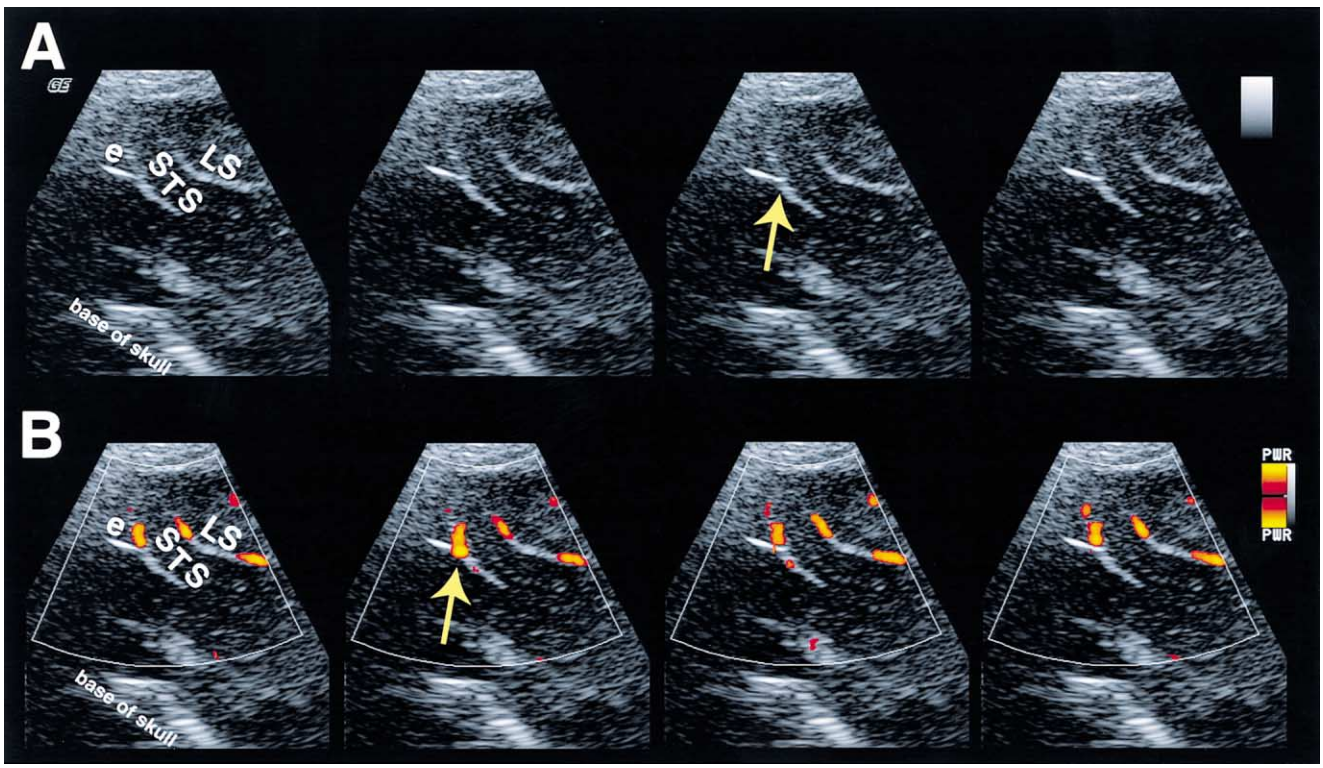

Fig. 4. Sonography during an electrolytic lesion. Time series of sonographic images of the STS, aligned as in Fig. 3, in an anesthetized macaque monkey. Moving from left to right the images show the electrode tip in 1 s time-steps immediately before and during an electrolytic lesion. (A) B-mode images of an electrode in area MT before (leftmost image) and as a 5 μA d.c. current was passed through the electrode. Note the region of increased reflectivity that grows in size during the five seconds of the lesion and then remains constant in size. The yellow arrow marks the lesion-associated area of high reflectivity once it has achieved maximal size. (B) Power doppler images, taken at the same time as the images shown in panel A. Note the transient increase in the power of the doppler spectra immediately after the current begins to flow through the electrode (yellow arrow). This increase in the power doppler spectra persists for less than 1 s. Abbreviations as in Fig. 3.

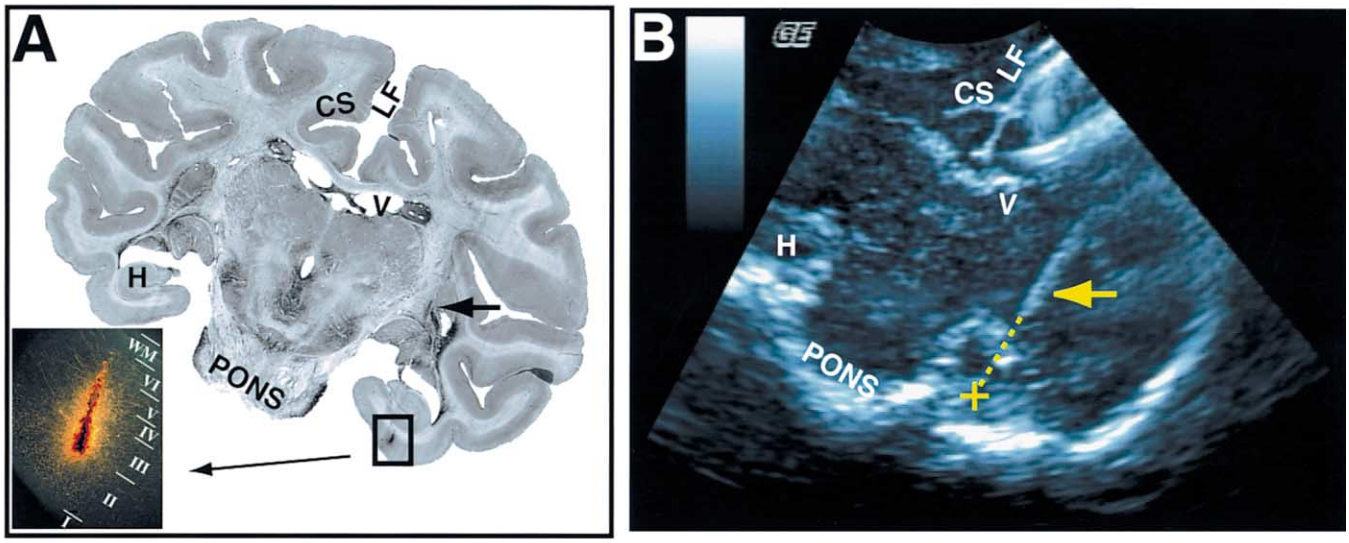

Fig. 5

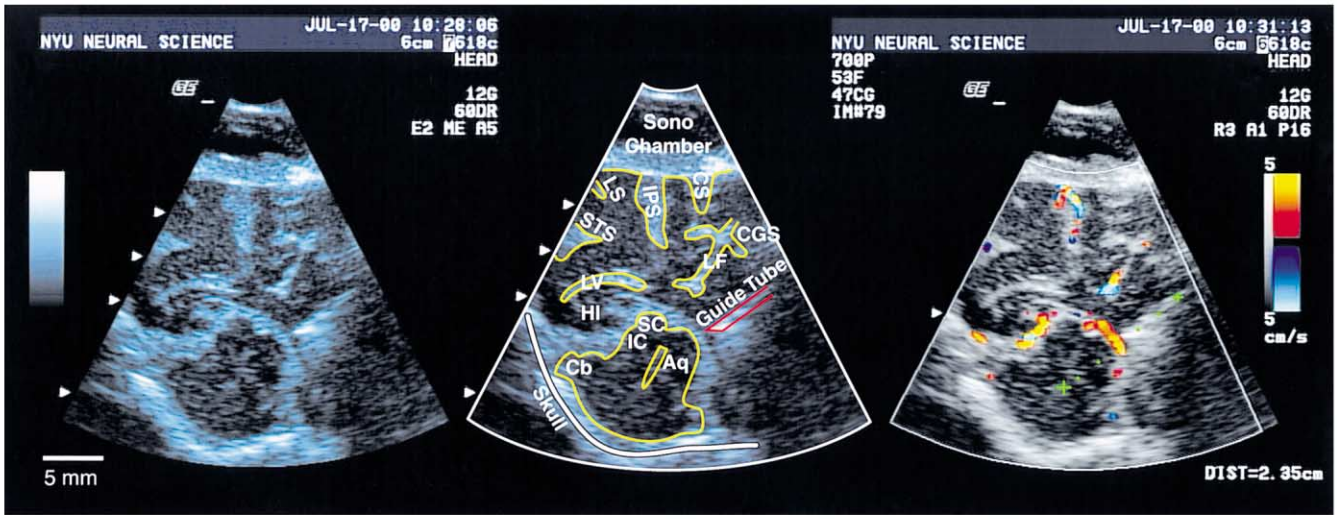

Fig. 6

Fig. 5. Sonography guiding anatomical tracer injection. Use of sonographic imaging to place deep brain neuroanatomical tracer injections is shown in this figure. A pulled micropipette was coated to within 10 mm of the injection tip with acrylic varnish and then lowered into parahippocampal cortex where a tracer injection was made. The left panel shows a coronal section through the injection site stained for BDA. The black arrow marks the track of the injection pipette. The injection site is shown at higher magnification in dark field on the left. The right panel shows the same coronal section imaged through a 10 mm × 15 mm craniotomy placed over the contraversive parietal cortex. The yellow arrow marks the acrylic coated micropipette. The dotted yellow line and cursor mark the extension of the pipette for exactly 10 mm to the presumed injection site. Abbreviations: CS, cingulate sulcus; H, hippocampus; LF, longitudinal fissure; V, lateral ventricle.

Fig. 6. Sonography guiding chronic primate electrophysiology. Use of sonographic imaging to place sonographically visible guide tubes for chronic recording in an awake-behaving monkey. The left panel plots a color enhanced B-mode image in the coronal plane at the level of the superior colliculus. The center panel replots this image with major structural boundaries outlined in yellow and labeled. Note the 22 gauge stainless steel guide tube on the right side of the image. The lower tip of the guide tube is placed about 1 mm above the superior colliculus on the right side. Note that the guide tube subtly compresses the colliculus on that side. The right panel plots blood flow rates towards and away from the probe in color. The green dotted line shows the approximate trajectory that would be taken by an electrode advanced out of the guide tube. The lower green cross shows the approximate point at which the electrode would cross the midline. On the lower right the sonograph prints the length of the green dotted line. Abbreviations: Aq, cerebral aqueduct; Cb, cerebellum; CGS, cingulate sulcus; CS, central sulcus; HI, hippocampus; IC, inferior colliculus; IPS, intraparietal sulcus; LS, lateral sulcus; LV, lateral ventricle; SC, superior colliculus; STS, superior temporal sulcus.

imaging as a research tool. Before using ultrasound to visualize a neurobiological probe in an anatomical structure one must identify the highest acoustic frequency that will penetrate the overlying tissue to image the anatomical structure of interest. One can then determine whether that frequency provides adequate resolution for the proposed experimental protocol. At the moment, commercial probes developed for use in hu-

man neonates are well adapted for imaging structures deep inside monkey brains. These probes, operating at frequencies around 7.5 MHz, can be used to localize electrodes and pipettes with sub-millimeter vertical accuracy at distances of up to 45 mm. Working in primates, this resolution permits the reliable placement of neurobiological probes within almost any anatomical structure of interest, although it does not permit intra-structural localization in most cases. Commercially available dermatological probes, operating at frequencies of up to 20 MHz, may be well suited to primate intra-structural imaging at depths of 1–2 cm or for deep brain imaging in smaller species. An experimental system developed by Turnbull and colleagues, which operates at frequencies of 50–60 MHz, has even been used as an ultrasonic microscope for near field imaging in fetal mouse brains where a resolution of ~ 50 μm has been achieved (Turnbull et al., 1995; Olson et al., 1997).

In order to achieve intra-structural accuracy for deep brain studies in larger animals like primates it may be possible to combine sonographic and magnetic resonance imaging techniques. Magnetic resonance images may soon be available with resolution approaching 150 μm. This resolution would allow neurobiologists to produce extremely detailed brain atlases for each experimental subject before any experiment was performed. Real-time sonography could then be used to align a moving visible probe with a stored magnetic resonance database and to compensate, in the stored database, for mechanical distortions of the brain produced by surgical procedures and introduced probes. The combined static magnetic resonance data and dynamic sonographic technology might offer both extremely high resolution and the ability to image probes in the laboratory setting at a low cost. While techniques for aligning the sonographic and magnetic resonance images are not yet fully developed, a preliminary clinical examination suggests that such an approach may be highly practical (Suhm et al., 1998).

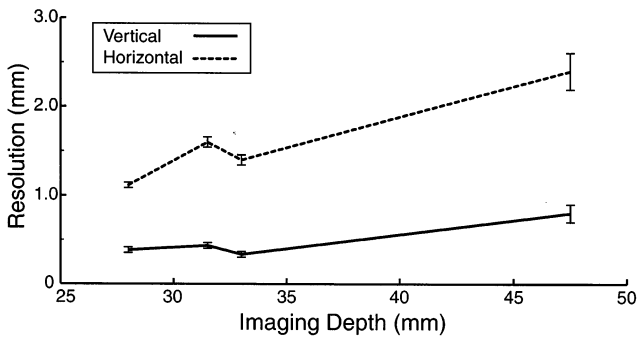

Fig. 7. Resolution as a function of depth. The image of a tungsten microelectrode was used to estimate the sonographic resolution we obtained as a function of depth. The data were gathered with a GE 618c probe. The machine was configured with a single depth focus aligned with the point on the microelectrode being imaged. Imaging center frequency was 7.5 MHz. The solid line plots the vertical (axial) resolution as a function of the depth of tissue through which the imaging pulse passed. The dashed line plots horizontal (lateral) resolution as a function of depth. See text for details.

Another benefit of sonographic imaging is that it permits the direct visualization of the neurovasculature. While this doppler shift-based visualization is at a resolution lower than that of regular B-mode imaging, we found that it allowed us to position neurobiological probes in ways that minimized vessel damage and thus minimized the incidence and severity of probe induced stroke. For our studies in the brainstem this is of particular importance because without sonographic guidance the placement of brainstem probes often results in severe vascular damage.

In most of the studies reported here we found that it was often difficult to maintain a precise alignment between the imaging plane of the probe and the axis of the neurobiological probe or electrode. Accurately extrapolating the trajectories of electrodes or pipette tips requires that the axis of the electrode or pipette lie entirely within the imaging plane. Images like those shown in Figs. 3 and 4, which are imperfectly aligned, make this limitation clear. The electrode is traveling across the plane of the image. While the location of the tip of the electrode is imaged accurately as lying just anterior to the parenchyma of the superior temporal sulcus, the precise tissue through which the electrode would pass on the posterior side of the sulcus is not shown in this image. Were the electrode advanced more than about 1.5 mm in this configuration it would pass out of the imaging plane. To address this limitation we are currently developing mechanical systems which insure that both electrode and probe operate within a common plane as shown in Fig. 5.

We encountered a number of less significant difficulties which, though easily overcome, are worth noting. When glass or metal probes are advanced perpendicular to the imaging axis of the probe, secondary reflections from the glass or metal probes become quite prevalent in the sonographic image. These are secondary echoes that appear as a vertical smearing or vertical sequential repetitions of the probe. The first, or highest, of these images is the actual location of the probe and the secondary echoes appear beneath it. We found that these secondary reflections were easy to control by adjusting the gain of the receiver and by decreasing the angle between the probe and the electrode, but they did occur under some circumstances. We also found that the size of the imaging aperture affected image quality. As the aperture became small with regard to the ultrasonic probe, resolution decreased and artifactual speckling appeared in the image, particularly on the sides of the image that lay beneath the edges of the aperture. Except for very near field imaging we found that craniotomies of less than 8 mm, or craniotomies with very irregular edges, produced unacceptable artifacting with our 12 mm wide probe. Finally, when we imaged through chroni-

cally implanted cylindrical access chambers we found that the material out of which the sonographic imaging chamber was fabricated had a significant impact on image quality. Metal access chambers produced a large number of artifactual echoes, principally in the near field, that obscured the sonographic image of the tissue. Plastic chambers, in contrast, produced notably fewer artifacts and thus yielded higher quality images.

The images presented here convey an overall sense of the resolution and utility of sonography in experimental neurophysiology and neuroanatomy. Sonography is, however, a dynamic technique. When operating at frame rates of 10–40 Hz, contemporary real-time ultrasonographs provide an experienced sonographer with significantly more information than is captured in still images. Observing probes in motion within the living brain, the active deformation of tissue by electrodes, and the pulsations of the neurovasculature provide a neurobiologist with data that is not well captured in this print article. The images presented here should be thought of as a starting point. These data show that the application of clinical sonographic imaging to neurobiological research can essentially eliminate the inter-structural uncertainty that has always plagued stereotaxic surgery and they suggest that future advances may permit the accurate intra-structural placement of probes under some conditions.

Over the past 12 months we have used ultrasonography to localize neurobiological probes on a daily basis. We have found that after 2–4 weeks of practice, with occasional supervision from an experienced sonographer, most investigators are able to easily identify anatomical structures and probes within the dynamic sonographic image. While many laboratories may choose to employ sonographs owned by others for brief periods, low-cost portable sonographs are now becoming available. These low-cost machines may make it possible for any laboratory to afford daily sonographic imaging. In our laboratory the techniques described here have nearly doubled the efficiency with which we conduct neurophysiological research and we believe that this gain in productivity could be realized by many neurophysiological and neuroanatomical scientists.

5. Web links

A more complete sonographic atlas of the macaque brain can be downloaded from our laboratory website. We also make available on the website several quicktime movies which show a lesion being made, single unit recordings being made, a three-dimensional reconstruction of the intraparietal sulcus in an awake behaving monkey, and doppler images of whole brain cerebral blood flow. All these images are available at http://www.cns.nyu.edu/ ~ glimcher.

Acknowledgements

The authors would like to acknowledge Dr. Richard Lipset of the St Lukes-Roosevelt Hospital Center in New York for critical early assistance and guidance. The financial assistance of the McKnight Foundation made this project possible. Professors J. Anthony Movshon and Wendy Suzuki, and their laboratory groups were invaluable and supportive colleagues. Professor Movshon's assistance was critical for producing the images shown here as Figs. 2 and 3. Professor Suzuki's assistance was critical for producing the images shown in Fig. 5. Finally, we would like to acknowledge the assistance of Dr. Deborah Ottenheimer of The Bronx-Lebanon Hospital in New York and Jerry Klunek of Toshiba America both of whom helped us to initiate this project.

References

Crist CF, Yamasaki DS, Komatsu H, Wurtz RH. A grid system and a microsyringe for single cell recording. J Neurosci Methods 1988;26:117–22.

Fitzgerald DE, Drumm. JE. Non-invasive measurement of human fetal circulation using ultrasound: a new method. Br Med J 1977:ii:1450–1451.

Fritsch GT, Hitzig E. On the electrical excitability of the cerebrum. In: Some papers on the cerebral cortex. Von Bonin, trans. Springfield, IL: Thomas: 1960. Originally in Archiv Anat Physiol Wiss Med 1870:300–332.

Gegenfurtner KR, Kiper DC, Beusmans JM, Carandini M, Zaidi Q, Movshon JA. Chromatic properties of neurons in macaque MT. Vis Neurosci 1994;11:455–66.

Gill RW, Kossof G. Quantitative blood flow measurements in deep-lying vessels. In: Chef R, editor. Real time ultrasound in perinatal medicine. Karger, 1977:139–41.

Glimcher PW, Platt ML, Ciaramitaro VM, Handel A, Brown MA, Bayer HM. Real-time ultrasonic imaging of neuroanatomical structure and single-unit electrodes in the living primate brain. Soc Neurosci Abstr 1999:25: 618.12.

Gordon D. Echoencephalographie. Rev Neurol 1958;9:652–3.

Handel A, Glimcher PW. A quantitative analysis of substantia nigra pars reticulata activity during a visually-guided saccade task. J Neurophysiol 1999;82:3458–75.

Horsley V, Clarke RH. The structure and functions of the cerebellum examined by a new method. Brain 1908;31:1–80.

Kikuchi T, Uchida R, Tanaka K, Wagai T. Early cancer diagnosis through ultrasonics. J Acoust Soc Amer 1957;29:824–33.

Kremkau FW. Diagnostic ultrasound. Philadelphia: Saunders, 1998.

Leksell L. Echo-encephalography: I. Detection of intracranial complications following head injury. Acta Chir Scand 1956;110:301–15.

Logothetis N. Can current fMRI techniques reveal the micro-architecture of cortex? Nat Neurosci 2000;3:413–4.

Olson M, Cambell K, abd Turnbull DH. Specification of mouse telencephalic and mid-hindbrain progenitors following heterotopic ultrasound-guided embryonic transplantation. Neuron 1997;19:761–72.

Platt ML, Glimcher PW. Responses of intra-parietal neurons to saccadic targets and visual distractors. J Neurophysiol 1997;78:1574–89.

Suhm N, Dams J, van Leyen K, Lorenz A, Bendl R. Limitations for three-dimesnional ultrasound imaging through a bore hole trepanation. Ultrasound Med Biol 1998;24:663–71.

Suzuki WA, Amaral DG. Perirhinal and parahippocampal corticies of the monkey: Cortical afferents. J Comp Neurol 1994;350:497–533.

Turnbull DH, Bloomfield TS, Baldwin HS, Foster FS, Joyner AL. Ultrasound backscatter microscope analysis of early mouse embryonic brain development. Proc Natl Acad Sci USA 1995;92:2239–43.

White DN, Curry GR. Absorption of ultrasonic energy by the skull. In: White DN, editor. Ultrasound in medicine I. New York:: Plenum, 1975.

White DN, Curry GR, Stevenson RJ. The acoustic characteristics of the skull. Ultrasound Med Biol 1978;4:225–52.